The Journal of Immunology

IPS-1 Signaling Has a Nonredundant Role in Mediating Antiviral Responses and the Clearance of Respiratory Syncytial Virus

Tine Demoor, Bryan C. Petersen, Susan Morris, Sumanta Mukherjee, Catherine Ptaschinski, Denise E. De Almeida Nagata, Taro Kawai, Toshihiro Ito, Shizuo Akira, Steven L. Kunkel, Matthew A. Schaller and Nicholas W. Lukacs

J Immunol 2012; 189:5942-5953; Prepublished online 7 November 2012;
doi: 10.4049/jimmunol.1201763
http://www.jimmunol.org/content/189/12/5942

The Journal of Immunology is published twice each month by
The American Association of Immunologists, Inc.,
1451 Rockville Pike, Suite 650, Rockville, MD 20852

Print ISSN: 0022-1767 Online ISSN: 1550-6606.

IPS-1 Signaling Has a Nonredundant Role in Mediating Antiviral Responses and the Clearance of Respiratory Syncytial Virus

Tine Demoor,* Bryan C. Petersen,* Susan Morris,* Sumanta Mukherjee,* Catherine Ptaschinski,* Denise E. De Almeida Nagata,* Taro Kawai,† Toshihiro Ito,‡ Shizuo Akira,† Steven L. Kunkel,* Matthew A. Schaller,* and Nicholas W. Lukacs*

The cytosolic RNA helicases melanoma differentiation–associated gene 5 and retinoic acid–inducible gene-I and their adaptor IFN-β promoter stimulator (IPS-1) have been implicated in the recognition of viral RNA and the production of type I IFN. Complementing the endosomal TLR, melanoma differentiation–associated gene 5, and retinoic acid–inducible gene-I provides alternative mechanisms for viral detection in cells with reduced phagocytosis or autophagy. The infection route of respiratory syncytial virus (RSV)—via fusion of virus particles with the cell membrane—points to IPS-1 signaling as the pathway of choice for downstream antiviral responses. In the current study, viral clearance and inflammation resolution were indeed strongly affected by the absence of an initial IPS-1–mediated IFN-β response. Despite the blunted inflammatory response in IPS-1–deficient alveolar epithelial cells, pulmonary macrophages, and CD11b$^+$ dendritic cells (DC), the lungs of RSV-infected IPS-1–knockout mice showed augmented recruitment of inflammatory neutrophils, monocytes, and DC. Interestingly, pulmonary CD103$^+$ DC could functionally compensate for IPS-1 deficiency with the upregulation of certain inflammatory cytokines and chemokines, possibly via TLR3 and TLR7 signaling. The increased inflammation and reduced viral clearance in IPS-1–knockout mice was accompanied by increased T cell activation and IFN-γ production. Experiments with bone marrow chimeras indicated that RSV-induced lung pathology was most severe when IPS-1 expression was lacking in both immune and nonimmune cell populations. Similarly, viral clearance was rescued upon restored IPS-1 signaling in either the nonimmune or the immune compartment. These data support a nonredundant function for IPS-1 in controlling RSV-induced inflammation and viral replication. *The Journal of Immunology*, **2012, 189: 5942–5953.**

Respiratory syncytial virus (RSV) causes severe respiratory tract infections in infants and immunocompromised patients. RSV has furthermore been shown to significantly contribute to the risk of asthma inception and exacerbation, yet the development of a safe and effective RSV vaccine is still work in progress. In addition to prophylactic intervention, therapeutic treatment should be optimized to control the inflammatory response against infection. It is therefore crucial to identify and characterize the initial proinflammatory signaling pathways that lead to the host's antiviral response.

*Department of Pathology, University of Michigan, Ann Arbor, MI 48109; †Laboratory of Host Defense, Department of Host Defense, WPI Immunology Frontier Research Center, Research Institute for Microbial Diseases, Osaka University, Osaka 565-0871, Japan; and ‡Department of Pathology and Experimental Medicine, Graduate School of Medicine, Dentistry, and Pharmaceutical Sciences, Okayama University, Okayama 700-8558, Japan

Received for publication June 25, 2012. Accepted for publication October 15, 2012.

This work was supported by National Institutes of Health Grants R01 HL059178 and R01 HL036302.

Address correspondence and reprint requests to Dr. Nicholas W. Lukacs, Department of Pathology, University of Michigan, 109 Zina Pitcher Place, 4059 Biomedical Science Research Building, Ann Arbor, MI 48109-2200. E-mail address: nlukacs@umich.edu

The online version of this article contains supplemental material.

Abbreviations used in this article: AEC, alveolar epithelial cell; BAL, bronchoalveolar lavage; BMDC, bone marrow–derived dendritic cell; BMMΦ, bone marrow–derived macrophage; DC, dendritic cell; dpi, day postinfection; IPS, IFN-β promoter stimulator; IRF, IFN regulatory factor; KO, knockout; MΦ, macrophage; MdA5, melanoma differentiation–associated gene 5; Nod2, nucleotide-binding oligomerization domain 2; pDC, plasmacytoid dendritic cell; PRR, pattern recognition receptor; RIG-I, retinoic acid–inducible gene-I; RSV, respiratory syncytial virus; WT, wild-type.

Upon virus entry and replication, viral components are first recognized by pattern recognition receptors (PRRs), generating an early defensive response: the production of type I IFNs. In the case of RSV, single-stranded and double-stranded viral RNA can be detected in the endosomal compartments by TLRs 7 and 3, respectively. TLR3 interacts with adaptor protein TRIF and TLR7 uses MyD88. The TLR3 and TLR7 pathway, respectively, activate the transcription factors IRF3 and IRF7, which induce the expression of type I IFNs IFN-β and IFN-α. Both pathways moreover activate the transcription factor NF-κB, hereby initiating the transcription of proinflammatory genes. In addition, the early type I IFN response will go on to generate the second phase of IFN transcription via autocrine and paracrine signals, reinforcing the expression of inflammatory cytokines/chemokines and allowing an adequate response against RSV. Indeed, we have previously demonstrated the importance of TLR3 and TLR7 expression in RSV-infected lungs. Deletion of TLR3 aggravated RSV-induced pulmonary disease with enhanced mucus production and the skewing of the Th response toward a Th2 cytokine profile (1), whereas a comparable mucogenic response in TLR7-deficient mice appeared driven by a Th17 response (2). Interestingly, viral clearance remained intact in the absence of TLR3 and TLR7, suggesting the involvement of additional signaling pathways in antiviral defense.

Notably, TLR activation in the endosomal compartment requires endocytosis of viral RNA molecules, phagocytosis of apoptotic infected cells or host cell autophagy. Because RSV particles enter the cell via fusion with the cell membrane, depositing their nuclear contents in the cytoplasm, the cytosolic PRRs nucleotide-binding oligomerization domain 2 (Nod2) and RNA helicases such as melanoma differentiation–associated gene 5 (MdA5) and retinoic

www.jimmunol.org/cgi/doi/10.4049/jimmunol.1201763

acid–inducible gene-I (RIG-I) are the alternative detectors likely to be engaged upon early infection. Accordingly, Nod2 expression has been shown to increase upon RSV infection and to mediate IFN-β production as well as viral clearance via ssRNA recognition (3). Moreover, RIG-I selectively recognizes dsRNA and 5′-triphosphate RNA (4, 5), characteristic for viral genomic RNA. Following viral RNA detection, Nod2, MdA5, and RIG-I all interact with the same adaptor, the IFN-β promoter stimulator (IPS-1) on the mitochondrial membrane (6). The resulting signal propagation will converge with the TLR3 pathway for the activation of IRF3 and NF-κB (7).

In this study, we characterized the importance of IPS-1 for the induction of antiviral responses using an established murine model of RSV-induced disease (8). Our results elaborate on previous reports, showing IPS-1–dependent type I IFN responses in RSV-infected fibroblasts and bone marrow–derived APCs (9, 10) along with IPS-1–mediated clearance of RSV (3, 10). In our experiments, we determined the role of IPS-1 in local orchestrators of RSV-induced lung inflammation: alveolar epithelial cells, alveolar and interstitial macrophages (MΦ), and pulmonary $CD11b^+$ dendritic cells (DCs) all appeared highly dependent of IPS-1 for their expression of cytosolic RNA helicases (Mda5 and RIG-I) and endosomal TLRs (TLR3 and TLR7) upon RSV infection. IPS-1 deficiency furthermore strongly dampened antiviral responses in these cell types, including the upregulation of type I IFNs and inflammatory cytokine/chemokines. Conversely, $CD103^+$ DCs could functionally compensate for the lack of IPS-1—potentially via TLR3 and TLR7 signaling—and increased their expression of IL-1β, CXCL1, and CCL2. Accordingly, absence of IPS-1 expression in vivo completely abolished the systemic and local RSV-induced IFN-β response and triggered exaggerated pulmonary inflammation, characterized by inflammatory monocytes, neutrophils, and $CD11b^+Ly6C^+$ DCs. Unexpectedly, delayed viral clearance in IPS-1–knockout (KO) mice was accompanied by increased T-cell activation and skewing toward a Th1 profile. Finally, bone marrow chimeras revealed the importance of IPS-1 signaling in nonimmune versus immune cells: a general lack of IPS-1 caused the most severe inflammation; similarly, viral clearance was rescued by IPS-1 expression in either hematopoietic or structural cells.

Materials and Methods

Animals

IPS-1 knockout mice were generated as previously described (11) and were provided by Dr. S. Akira (Osaka University, Osaka, Japan) to start a breeding colony at the University of Michigan animal facilities. Wild-type (WT) C57BL/6 controls were purchased from Taconic Farms (Germantown, NY). All animal work was approved by the University Committee on Use and Care of Animals.

Respiratory syncytial virus

The Line 19 strain, originally isolated from a sick infant at the University of Michigan Hospital, is propagated in our laboratory in HEp-2 cells (American Type Culture Collection). Line 19 elicits disease in mice comparable to severe RSV infection in humans, including significant airway hyperresponsiveness and mucus overproduction (12). Mice were anesthetized and infected intratracheally with 1×10^5 PFU/animal.

Bronchoalveolar lavage

The bronchoalveolar space was lavaged via a tracheal cannula, instilling 3×300 μl, followed by 3×1 ml 1% BSA PBS, free of ionized calcium and magnesium. The three small fractions were collectively centrifuged for cytokine measurement in the supernatant. Subsequently, cell pellets from all lavage fractions were pooled and resuspended in 1 ml 1% FCS PBS. A total cell count was performed with a Z2 Beckman Coulter particle counter (Beckman Coulter, Indianapolis, IN), and differential cell counts (on at least 400 cells) were performed on cytospins stained with Diff-Quick reagents (Siemens, New York, NY). The rest of the BAL cells were analyzed with flow cytometry.

Culture and stimulation of lymph node cells, alveolar epithelial cells, DCs, and MΦ

Mediastinal lymph nodes were digested mechanically, by use of 18-gauge needles and enzymatically, via incubation with 1 mg/ml collagenase A (Roche, Indianapolis, IN) and DNase I (Sigma-Aldrich, St. Louis, MO) in RPMI 1640 with 10% FCS. Following RBC lysis, cells were passed through a 40-μm strainer and counted with a Z2 Beckman Coulter particle counter. Suspensions of total lymph node cells were cultured in complete medium and restimulated with RSV during 48 h for Th cytokine measurements in the culture supernatant. The rest of the lymph node cells were analyzed with flow cytometry.

Bone marrow was flushed from femur and tibia bones. Dendritic cells were grown from bone marrow progenitor cells in complete medium with 10 ng/ml GM-CSF (R&D Systems, Minneapolis, MN) with medium changes on days 5 and 7. By day 10, 90–95% of the cell population is $CD11c^{hi}CD11b^{hi}MHCII^+$, as determined by flow cytometry. To obtain MΦ, bone marrow cells were cultured in L929 cell-conditioned medium, as described previously. On day 7, flow cytometric analysis showed 85–90% of the cells to be $CD11c^+CD11b^{hi}F4/80^+MHCII^{med}Gr1^-$ with high forward scatter. The procedure to harvest the different APCs from the lung is illustrated in Supplemental Fig. 1. First, airways from naive mice were lavaged as described above to isolate alveolar MΦ. Next, the lungs were digested, and $CD11c^+$ cells were enriched from lung single-cell suspensions using MACS MicroBeads (Miltenyi Biotec). Subsequently, pulmonary MΦ were sorted as $CD11c^{hi}$ cells with high autofluorescence, $CD11b^+$ DCs as low autofluorescent $CD11c^{hi}MHCII^+CD11b^{hi}CD103^-$ cells, and $CD103^+$ DCs as low autofluorescent $CD11c^{hi}MHCII^+CD11b^{lo}CD103^+$ cells, using a FACSAria II cell sorter (BD Biosciences).

Alveolar epithelial cells were cultured according to a previously described protocol (13). Subsequent steps involved the instillation of dispase and agarose via a tracheal cannula, followed by thorough mincing of the lungs and incubation with DNase I. Contaminating leukocytes were removed using biotinylated anti-CD32 and anti-CD45 Abs (BD Pharmingen, San Jose, CA) and streptavidin-coated magnetic beads. Cell viability was >97% by trypan blue exclusion. Cell suspensions were incubated in petri dishes overnight to remove residual adherent mesenchymal cells. Nonadherent cells stained >99% positive for pro-surfactant protein C and were plated on fibronectin-coated 24-well plates in DMEM (Life Technologies, Grand Island, NY) supplemented with 10% FCS (5×10^5 cells/well). After 3 d of culture, cells were found to be >95% vimentin negative.

Primary alveolar epithelial cell cultures, bone marrow–derived DCs (BMDCs), and bone marrow–derived MΦ (BMMΦ) were infected with RSV for 12 h before extraction of RNA or for 24 h to measure protein in the culture supernatant.

mRNA extraction, reverse transcription, and RT-PCR

mRNA was isolated from ground up lung tissue and cell cultures using TRIzol reagent (Invitrogen, Carlsbad, CA) or the RNeasy Mini kit (Qiagen, Germantown, MD), according to the manufacturer's instructions. Five micrograms of RNA per sample was reverse transcribed using murine leukemia virus RTase (Applied Biosystems, Foster City, CA). Expression of MdA5, RIG-I, IPS-1, IL-1β, IL-4, IL-5, IL-6, IL-13, IL-17a, IFN-γ, CXCL1, CCL2, CCL3, CCL5, and CCL20 was analyzed with TaqMan gene expression assays (Applied Biosystems) using an ABI Prism 7500 Sequence Detection System (Applied Biosystems). Primers for IFN-α, IFN-β, TLR3 and TLR7, and RSV F, G, and N proteins were custom-made. Gene expression was normalized to GAPDH and expressed as fold change over the gene expression in control mice.

Protein measurement

Levels of Th cytokines, IL-4, IL-5, IL-13, IFN-γ, and IL-17 were determined in culture supernatant using a Bio-Plex assay (Bio-Rad). IFN-α and IFN-β protein were analyzed in serum, BAL fluid and culture supernatant with the VeriKine mouse IFN-α and IFN-β ELISA kits (PBL IFNSource).

Flow cytometry

Following FcR blocking, single-cell suspensions of bronchoalveolar lavage (BAL), lung, and lymph node cells were stained with anti-CD11c (N418), anti-Ly6C (HK1.4), anti-Ly6G (1A8; BioLegend, San Diego, CA), anti-CD11b (M1/70), anti-CD103 (2E7), anti-plasmacytoid dendritic cell Ag 1 (PDCA-1; eBioscience, San Diego, CA), and anti–MHC-II/IAb (AF6-120.1; BD Biosciences, San Jose, CA). Inflammatory neutrophils were gated as low autofluorescent, $CD11c^{lo}CD11b^{hi}Ly6C^+Ly6G^+$ with low forward scatter. Inflammatory monocytes were analyzed as low autofluorescent, $CD11c^{lo}CD11b^{hi}Ly6C^+Ly6G^-$ cells with low forward scatter. $CD11b^+$ DCs

were defined as low-autofluorescent $CD11c^{hi}MHCII^{+}CD11b^{hi}CD103^{-}$ cells; within this population, $Ly6C^{+}$ cells were considered to be inflammatory $CD11b^{+}$ DCs. $CD103^{+}$ DCs were defined as low-autofluorescent $CD11c^{hi}MHCII^{+}CD11b^{lo}CD103^{+}$ cells. Plasmacytoid DCs (pDCs) were defined as $PDCA\text{-}1^{+}$ cells within the low-autofluorescent $CD11c^{med}/MHCII^{med/lo}$ population, as described previously (14). CD86 expression was analyzed as a marker for activation of conventional and pDCs using anti-CD86 (clone GL-1) or isotype control rat IgG2a,κ (both from BioLegend).

For intracellular cytokine staining, lymph node cell suspensions were restimulated for 6 h in complete medium containing 0.5 μl/ml GolgiPlug, 0.5 μl/ml GolgiStop (BD Biosciences), 0.5 ng/ml PMA, and 500 ng/ml ionomycin. Subsequently, lymph node cells were first stained for surface markers with anti-CD3 (17A2), anti-CD4 (RM4-5) and anti-CD8 Abs (16-10A1; BioLegend), and anti-CD69 Ab (H1.2F3; eBioscience). Cells were then fixed with 4% formaldehyde and permeabilized (BD Biosciences Fix/Perm Kit) for incubation with anti–IFN-γ Ab (BD Pharmingen) or isotype control rat IgG1,κ (BD Pharmingen). T cells were defined as CD3-positive cells with low forward and side scatter and subdivided into CD4 or CD8 single-positive subpopulations.

Histology

The left lung was perfused with 4% formaldehyde for fixation and embedded in paraffin. Five-micrometer lung sections were stained with periodic acid-Schiff and hematoxylin to detect mucus production and inflammatory infiltrates. Photomicrographs were captured using a Zeiss Axio Imager Z1 and AxioVision 4.8 software (Zeiss, Oberkochen, Germany). Two independent blinded observers evaluated hematoxylin-stained lung sections for inflammatory infiltration around the bronchovascular bundles, using the following scoring system: 0, absent; 1, minimal; 2, slight; 3, moderate; 4, strong; and 5, severe.

Plaque assay

For the immunoplaque assay, total lungs were homogenized, and serial dilutions of the supernatant were incubated in a 24-well plate with Vero cell monolayers in Eagle's MEM and overlaid with methylcellulose, as described previously (15). After 4 d, incubation was stopped, and viral plaques were visualized using goat anti-RSV polyclonal Ab (Millipore, Temecula, CA).

Bone marrow chimeras

For bone marrow chimera experiments, recipient WT C57BL/6 mice and IPS-1 KO mice (6–8 wk old) were irradiated at 900 rad. Donor bone marrow was isolated from femurs and tibias of WT and IPS-1 KO mice. Via tail vein injection of 2×10^6 bone marrow cells in 100 μl RPMI 1640, the following bone marrow chimeras were created (donor → host): WT → WT, IPS-1 KO → WT, IPS-1 KO → IPS-1 KO, and WT → IPS-1 KO. 8 wk after reconstitution, bone marrow chimeras were infected with RSV.

Statistical analysis

Reported values are expressed as mean ± SEM. Statistical analysis was performed with GraphPad Prism software for Mac OS X version 5.0d (GraphPad Software, San Diego, CA) using nonparametric tests (Kruskall-Wallis; Mann-Whitney) or *t* tests in the case of Gaussian distribution. A two-tailed $p < 0.05$ was considered significant.

Results

The cytosolic RNA helicases Mda5 and RIG-I and their adaptor IPS-1 are increased following RSV infection; RSV induces IFN-β in an IPS-1–dependent manner

Our previous observations on RSV-induced expression of viral RNA detectors, including TLR3 and TLR7 (1, 2), motivated further investigation of the Mda5/RIG-I detection system. Using a time course of RSV infection in WT C57BL/6 mice, transcription of Mda5 was rapidly and strongly induced in lungs of RSV-exposed animals, starting at 1 d postinfection (dpi) and maintaining high plateau levels for at least 12 dpi (Fig. 1A). The RSV-induced regulation of RIG-I and IPS-1 showed a different pattern, with maximal induction at 4–6 dpi and normalization starting 8 dpi. Monitoring the expression of the Mda5/RIG-I-IPS-1 system in primary cultures of alveolar epithelial cells (AECs), BMDCs, and BMMΦ, we observed that all cell types responded to RSV infection with the upregulation of Mda5 and RIG-I, whereas only AECs showed a modest increase in IPS-1

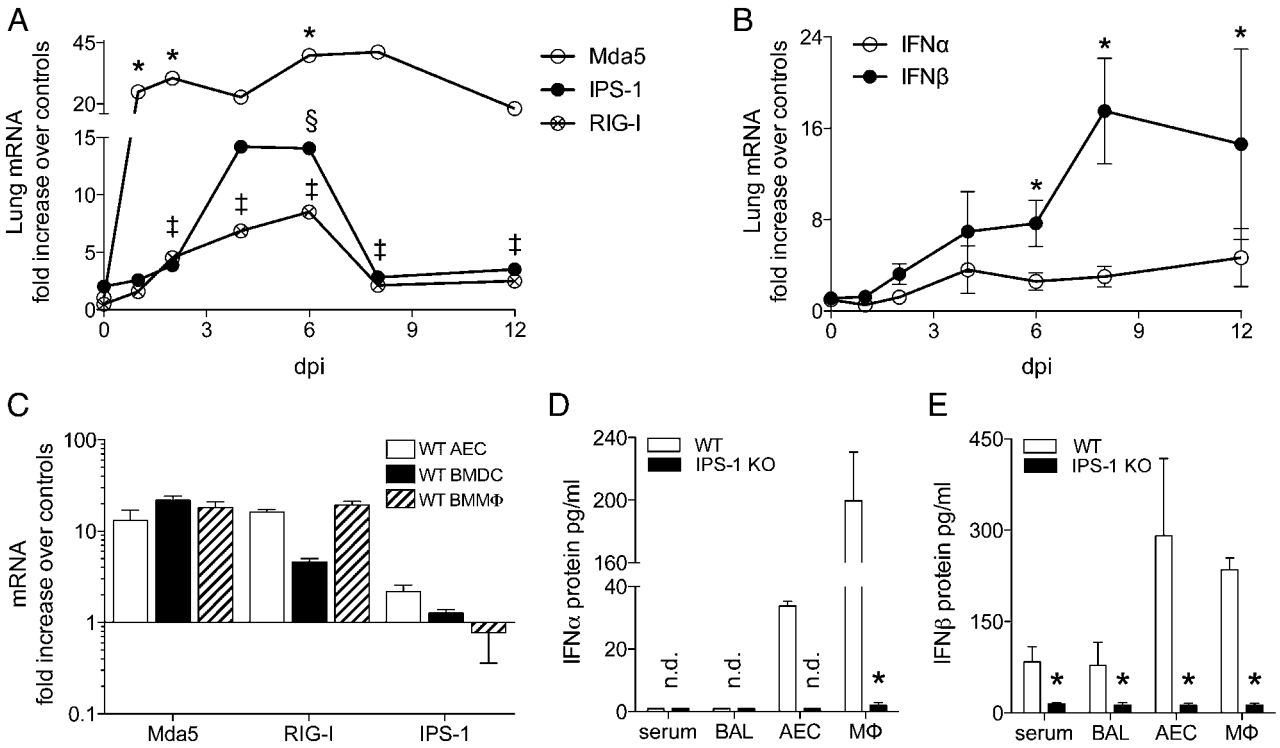

FIGURE 1. The cytosolic RNA helicases MDA5 and RIG-I and their adaptor IPS-1 are increased following RSV infection, RSV induces IFN-β in an IPS-1–dependent manner. mRNA expression of Mda5, RIG-I, and IPS-1 (**A**), mRNA expression of IFN-α and IFN-β (**B**) in total lung tissue of RSV-infected C57BL/6 mice at 1, 2, 4, 6, 8, and 12 dpi, determined by RT-PCR (expressed as fold increase over controls; mean ± SEM; $n = 4$–5). $*,\S,\ddagger p \leq 0.05$. (**C**) RSV-induced mRNA expression of Mda5, RIG-I, and IPS-1 in primary AEC cultures, , and BMMΦ of C57BL/6 mice, determined 12 h postinfection by RT-PCR (expressed as fold increase over controls; mean ± SEM; $n = 4$–5). RSV-induced IFN-α (**D**) and IFN-β (**E**) protein in serum and BAL fluid of WT and IPS-1 KO mice at 8 dpi and in primary cultures of AEC and sorted pulmonary MΦ at 1 dpi (expressed as picograms per milliliter; mean ± SEM; $n = 4$–5). $*p < 0.05$.

mRNA (Fig. 1C). The RSV-induced expression of Mda5 and RIG-I, both IFN-stimulated genes, indicated IRF3 activation and enhanced host detection of RSV.

The local type I IFN response (IFN-α and IFN-β) in the lung demonstrated a rapid induction of IFN-β in RSV-exposed animals as early as 2 dpi (Fig. 1B). Local (in the BAL fluid) and systemic (in the serum) protein levels of IFN-β in RSV-infected animals were highly dependent of IPS-1 expression (Fig. 1E). To better understand the nature of the reduced local and systemic levels, IFN-β production was also examined in isolated cell populations. Whereas IFN-β production was below detection limit in culture supernatant of BMDCs and BMMΦ (data not shown), AECs and sorted pulmonary (interstitial) MΦ (MΦ) were important sources of IPS-1–induced IFN-β (Fig. 1E). In contrast, IFN-α expression was only moderately upregulated (Fig. 1B). We could not detect any IFN-α protein in either serum or BAL fluid of RSV-infected mice at 8 dpi. Whereas cell-specific responses may be diluted in total lung tissue, AECs and interstitial MΦ responded to RSV infection with IPS-1–dependent IFN-α secretion (Fig. 1D). RSV did not alter IFN-α expression in the lung-draining (mediastinal) lymph nodes, whereas mRNA levels of IFN-β were increased by 12 dpi (Supplemental Fig. 2A). The increased IFN-β response following RSV infection suggests selective IRF3 activation by the IPS-1 signaling pathway.

Decreased inflammation resolution and viral clearance in RSV-infected IPS-1 KO mice

The importance of the different intracellular viral detectors during RSV infection has been demonstrated in previous studies, using TLR-deficient mice. Knocking out TLR3 and TLR7 significantly worsens RSV-induced lung pathology but leaves viral clearance intact (1, 2). Because RSV enters the cell via membrane fusion, cytosolic detection of the virus may be essential for early and effective antiviral responses, prompting further exploration of IPS-1 signaling upon RSV infection. For this purpose, we infected both WT and IPS-1 KO mice with RSV and compared their inflammation and antiviral defense at 8 dpi, because IFN-β expression was maximally induced at this time point in the lungs (Fig. 1B). Airway inflammation was evaluated via flow cytometric analysis of the cell populations in the BAL fluid. Whereas the airway compartment of naive WT and IPS-1 KO mice mainly contained

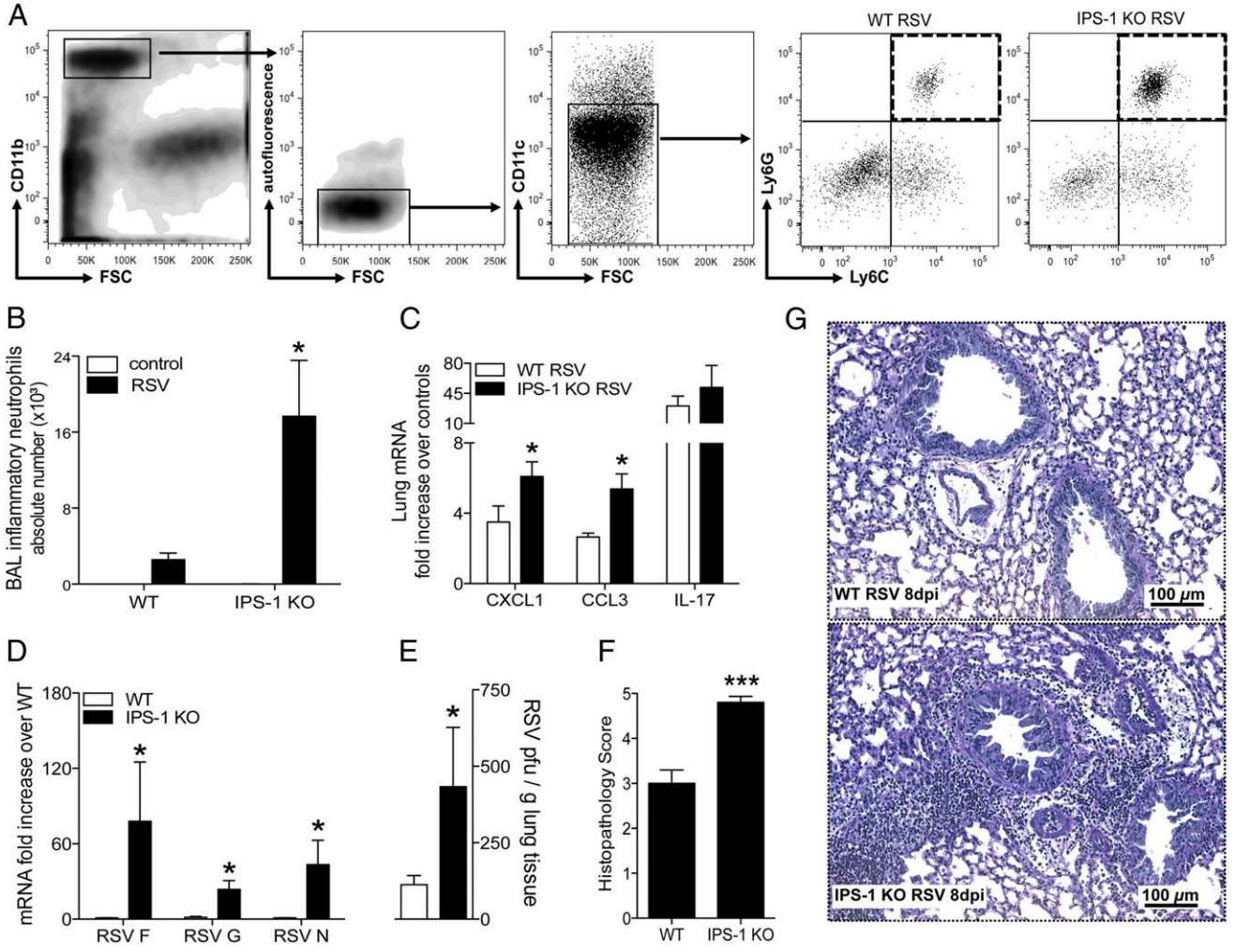

FIGURE 2. Decreased inflammation resolution and viral clearance in the absence of IPS-1. (**A**) Gating strategy for flow cytometric analysis of inflammatory neutrophils ($CD11b^{hi}$ with low forward scatter, low-autofluorescent $CD11c^{lo}Ly6C^{+}Ly6G^{hi}$, shown in the dashed quadrant). (**B**) Absolute numbers of inflammatory neutrophils in the BAL fluid of naive and RSV-infected WT and IPS-1 KO mice, determined by flow cytometry at 8 dpi. (**C**) RSV-induced mRNA expression of CXCL1, CCL3, and IL-17 in lungs of WT and IPS-1 KO mice, determined by RT-PCR at 8 dpi (expressed as fold increase over controls). (**D**) mRNA expression of the RSV F protein, G protein, and N protein in lungs of RSV-infected WT and IPS-1 KO mice, as determined by RT-PCR at 8 dpi (expressed as fold increase over RSV-infected WT). (**E**) RSV titers in lungs of WT versus IPS-1 KO mice, determined by plaque assay on day 3 postinfection (expressed as plaque forming units/ml). Histopathology scores (**F**) and representative photomicrographs (**G**) of hematoxylin-stained lung sections of WT and IPS-1 KO mice at 8 dpi. All data are expressed as mean ± SEM, $n = 5$. $^{*}p < 0.05$, $^{***}p < 0.001$.

MΦ (data not shown), RSV infection increased the number of inflammatory neutrophils (defined as low forward light scatter, $CD11b^{hi}$, low autofluorescent, $CD11c^{lo}Ly6C^{+}Ly6G^{hi}$; Fig. 2A). Compared with WT mice, RSV-infected IPS-1 KO mice exhibited significantly worse airway neutrophilia (Fig. 2B), accompanied by higher pulmonary expression of the neutrophil chemo-attractants CXCL1 and CCL3 (Fig. 2C).

In addition to the bronchoalveolar space, we analyzed lung tissue to verify whether the observed airway inflammation in RSV-infected IPS-1 KO mice could be associated with increased interstitial inflammation. As previously described, RSV-induced inflammatory cell infiltrates were rapidly cleared in WT C57BL/6 mice by 8 dpi (Fig. 2G). In IPS-1 KO mice, however, hematoxylin-stained lung sections still showed significant peribronchiolar inflammation at 8 dpi. Accordingly, RSV-infected IPS-1 KO mice received a significantly higher histopathology score (4.8 ± 0.13; severe) compared with WT mice (3.0 ± 0.29; moderate) (Fig. 2F). As illustrated by photomicrographs and histopathology scores in Supplemental Fig. 3, the degree of peribronchiolar inflammation is very similar between WT and IPS-1 KO mice at earlier time points (2 and 6 dpi) and does not differ in severity until 8 dpi, suggesting delayed resolution of RSV-induced inflammation. Overall mucus production did not differ between WT and IPS-1 KO mice (data not depicted). In agreement with the histology, lungs of RSV-infected IPS-1 KO contained more mRNA for the RSV F, G, and N proteins at 8 dpi (Fig. 2D), suggesting increased viral replication and/or diminished clearance. Therefore, we performed a plaque assay on day 3 postinfection and found significantly more virus in IPS-1 KO mice compared with WT mice (Fig. 2E). Thus, dysregulation of the early IFN-β response in IPS-1 KO mice leads to more severe RSV-induced inflammation and adversely affects virus elimination.

Increased numbers and activation of inflammatory-type $CD11b^{+}$ DCs in lungs of RSV-infected IPS-1 KO mice

Via flow cytometric analysis, we also compared DC numbers and activation (evaluated by CD86 expression) between controls and RSV-infected animals of both genotypes at 8 dpi (Fig. 3). We discriminated between the two main populations of conventional DCs in the lung ($CD11b^{+}$ versus $CD103^{+}$ DCs), using the gating strategy shown in Supplemental Fig. 1. 8 dpi with RSV, $CD11b^{+}$ DCs remained significantly increased in lungs of both WT and IPS-1 KO mice (Fig. 3A). Interestingly, only IPS-1 KO $CD11b^{+}$ DCs exhibited a remarkable CD86 expression compared with their WT counterparts. Whereas RSV infection did not significantly affect $CD103^{+}$ DC numbers, this population was still moderately activated at 8 dpi in both WT and IPS-1 KO mice (Fig. 3B).

pDCs reportedly generate their IFN-α response against single-stranded RNA viruses via TLR7 and MyD88 signaling and not via the RIG-I system (16–18). Moreover, IFN-α is not greatly induced upon infection with RSV strain Line 19 (Fig. 1B, 1D; Supplemental Fig. 2). Nonetheless, we determined pDC numbers in lungs and mediastinal lymph nodes of both WT and IPS-1 KO mice following RSV infection (Supplemental Fig. 4). As previously described (14), pDCs were defined as $PDCA\text{-}1^{+}$ cells within the low-autofluorescent $CD11c^{med}/MHCII^{med/lo}$ population (Supplemental Fig. 4A). At 8 dpi, the percentage and absolute number of pDCs were significantly increased in lungs of WT mice but not in IPS-1 KO mice (Supplemental Fig. 4B), whereas pDC numbers were increased in the lung-draining lymph nodes of mice of both genotypes (Supplemental Fig. 4C). Regardless of IPS-1 expression or RSV infection, pulmonary pDCs hardly expressed any CD86 (Supplemental Fig. 4B). Conversely, CD86 expression was detected on pDCs in lymph nodes of naive WT and IPS-1 KO controls (Supplemental Fig. 4C). Following RSV infection, the average CD86 expression on pDCs is significantly downregulated in the lymph nodes of both WT and IPS-1 KO mice.

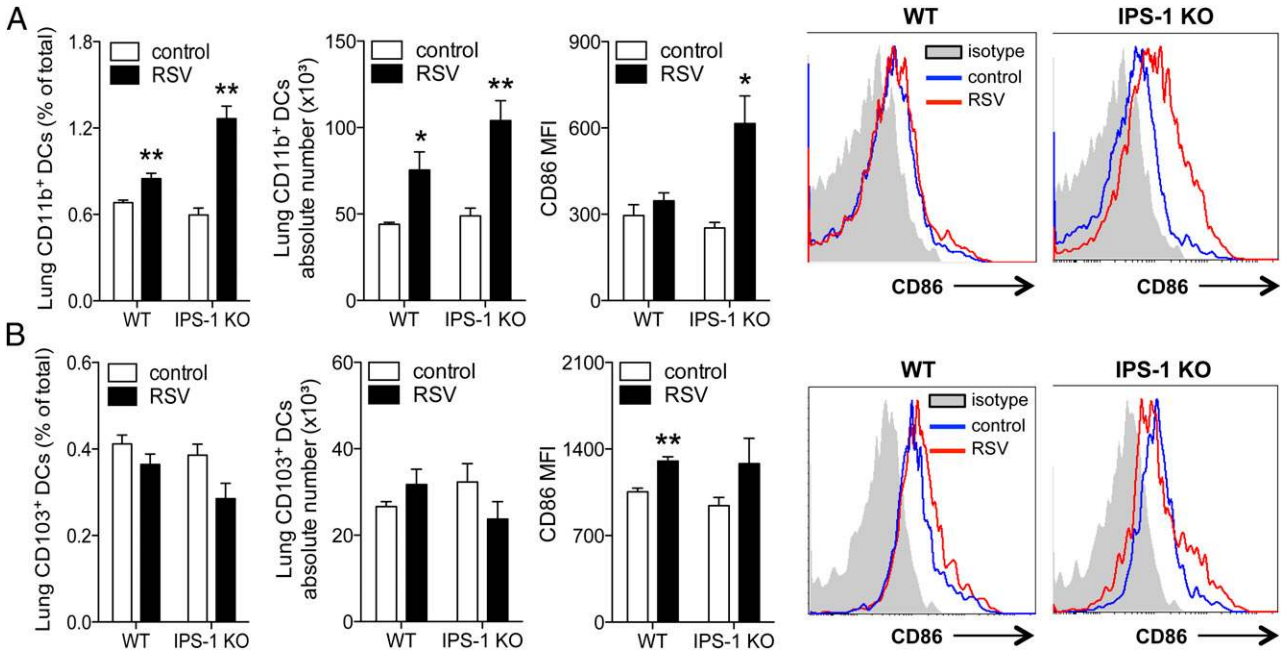

FIGURE 3. Increased numbers and activation of inflammatory-type $CD11b^{+}$DCs in lungs of RSV-infected IPS-1 KO mice. (**A**) Flow cytometric analysis of percentage and absolute numbers of pulmonary $CD11b^{+}$DCs ($CD11c^{hi}MHCII^{+}CD11b^{hi}CD103^{-}$ cells with low autofluorescence) at 8 dpi; relative mean fluorescent intensities (MFI) for CD86 expression on $CD11b^{+}$DCs (MFI Ab corrected for MFI isotype control), and representative histograms for naive and RSV-infected WT and IPS-1 KO mice at 8 dpi. (**B**) Percentage and absolute numbers of pulmonary $CD103^{+}$DCs ($CD11c^{hi}MHCII^{+}CD11b^{lo}CD103^{+}$ cells with low autofluorescence) at 8 dpi; MFI for CD86 expression on $CD103^{+}$DCs (MFI Ab corrected for MFI isotype control) and representative histograms. All data are expressed as mean ± SEM, $n = 4$–5. $^{*}p < 0.05$, $^{**}p < 0.01$.

RSV-infected IPS-1 KO mice have increased numbers and activation of T-cells with a predominant Th1 profile

Next, we verified whether the severe inflammation and hampered virus clearance in IPS-1 KO mice could be explained by altered antiviral T cell responses in the lungs and draining lymph nodes (Fig. 4). The proportion of activated ($CD69^+$) $CD4^+$ and $CD8^+$ T cells was significantly higher in lungs of IPS-1 KO mice compared with WT mice at 8 dpi (Fig. 4B, 4C). Moreover, significant IFN-γ protein levels could only be detected in the BAL fluid of RSV-infected IPS-1 KO mice (Fig. 4A). Upon RSV infection, total lymph node cell numbers gradually increased in both WT and IPS-1 KO mice (Fig. 4D). In accordance with the lung data, flow cytometric analysis of lymph node $CD4^+$ and $CD8^+$ T cells showed both populations to be increased in number and state of activation in IPS-1 KO mice compared with WT mice (Fig. 4F, 4G; absolute numbers can be found in Supplemental Fig. 2B-E). When cultured and restimulated with virus, IPS-1–deficient lymph node cells exhibited a Th1 phenotype: cell culture supernatants of IPS-1 KO mice contained more IFN-γ protein, but lower levels of Th2 cytokines—IL-4 and IL-5—and decreased Th17 cytokine IL-17 (Fig. 4E). We additionally confirmed the IFN-γ response in IPS-1 KO mice via flow cytometric analysis of the lymph node T cells: intracellular staining for IFN-γ revealed that both $CD8^+IFN\gamma^+$ and $CD4^+IFN\gamma^+$ T cells were increased in number in IPS-1–deficient lymph nodes upon RSV infection, as illustrated by representative histograms (Fig. 4F, 4G).

IPS-1 signaling mediates RSV-induced expression of cytokines, chemokines, and PRRs in the APCs of the lung

Despite the blunted IFN-β response, RSV-induced inflammation in IPS-1 KO mice was characterized by exaggerated recruitment,

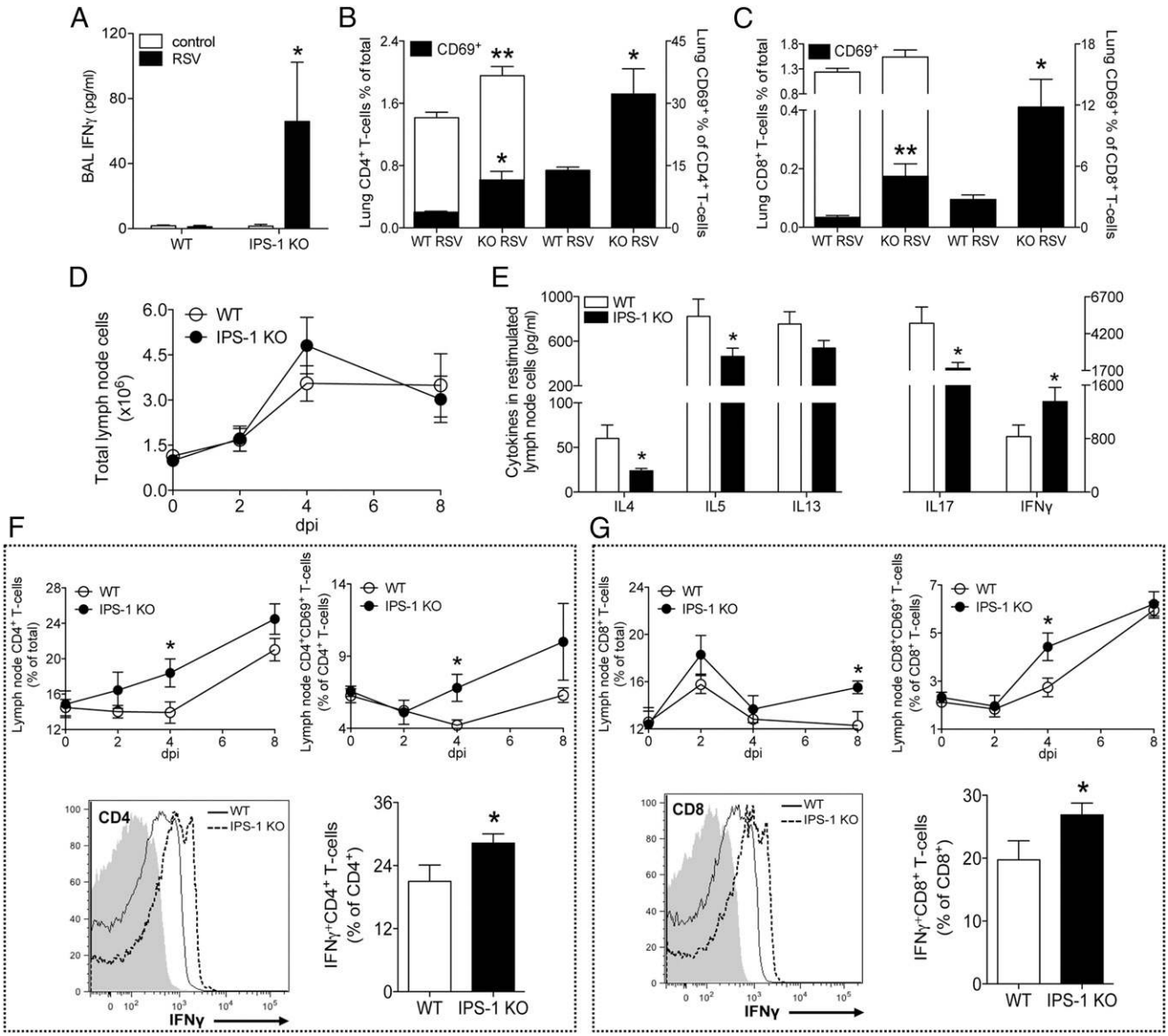

FIGURE 4. RSV-infected IPS-1 KO mice have increased numbers and activation of T cells with a predominant Th1 profile. (**A**) Protein levels of IFN-γ in BAL fluid of WT and IPS-1 KO mice, in a naive state and at day 8 post-RSV infection, measured by ELISA (expressed as picograms per milliliter). Numbers of total and activated ($CD69^+$) $CD4^+$ (**B**) and $CD8^+$ T cells (**C**) in lungs of RSV-infected WT and IPS-1 KO mice at 8 dpi. (**D**) Total cell numbers in mediastinal lymph nodes of WT and IPS-1 KO mice at 2, 4, and 8 dpi. (**E**) Th cytokine protein levels in lymph node culture supernatants after 48 h restimulation with RSV, as measured with a Bio-Plex assay (expressed as picograms per milliliter). (**F**) Overview of the $CD4^+$ T cell responses in lymph nodes of RSV-infected WT versus IPS-1 KO mice, including total $CD4^+$ T cell numbers, activated $CD4^+CD69^+$ T cell numbers, representative histograms illustrating positive IFN-γ signal within the $CD4^+$ T cell population and the number of $IFN\gamma^+CD4^+$ T cells, determined by flow cytometry. (**G**) Overview of the $CD8^+$ T-cell responses. All data are expressed as mean ± SEM; $n = 5$. $^*p < 0.05$, $^{**}p < 0.01$.

accumulation, and activation of inflammatory cells. Therefore, we determined the role of IPS-1 in different pulmonary cell populations, known to be targeted by RSV and to produce inflammatory cytokines and chemokines (Fig. 5). We established primary cultures of isolated AECs, alveolar and interstitial MΦ and CD11b$^+$ and CD103$^+$ DCs. Following RSV infection, we analyzed the type I IFN response, along with the induction of inflammatory cytokines and chemokines in cells derived from WT versus IPS-1 KO lungs. Furthermore, we quantified the RSV-induced expression of the cytosolic RNA helicases MdA5 and RIG-I versus the endosomal RNA detectors TLR3 and TLR7 in these different cell types. As illustrated in Fig. 5A, the IPS-1 pathway is crucial for the upregulation of IFN-β and inflammatory cyto/chemokines in the alveolar epithelium. IFN-β, IL-1β, IL-6, CXCL1, and CCL2 were all strongly increased upon RSV infection in WT cells but not in IPS-1 KO cells. The same was true for both alveolar and interstitial MΦ (Fig. 5B, 5C). Looking at more specialized APCs in the lung, pulmonary CD11b$^+$ DCs also depended on IPS-1 signaling for their RSV-induced expression of IFN-β, IL-6, CXCL1, and CCL2 (Fig. 5D). Alveolar MΦ, interstitial MΦ, and CD11b$^+$ DCs all responded to the virus with strong IFN-α expression in an IPS-1–mediated fashion. In contrast, IFN-α mRNA was modestly induced in virus-infected AECs and CD103$^+$ DCs but in an IPS-1–independent manner. Considering the predominant IFN-β response in RSV-infected lungs (Fig. 1B), the more abundant AECs appear to determine the local type I IFN profile.

In accordance with the IPS-1–dependent expression of cytokines and chemokines in RSV-infected AECs, pulmonary MΦ, and CD11b$^+$ DCs, the rapid induction of PRRs Mda5, RIG-I, TLR3, and TLR7 upon RSV infection of these cell types was also hampered in the absence of IPS-1 (Fig. 5F). Reportedly, TLR3 induction in RSV-infected airway epithelial cells indeed depends on IPS-1–mediated IFN-β secretion (19), and Mda5 and RIG-I have

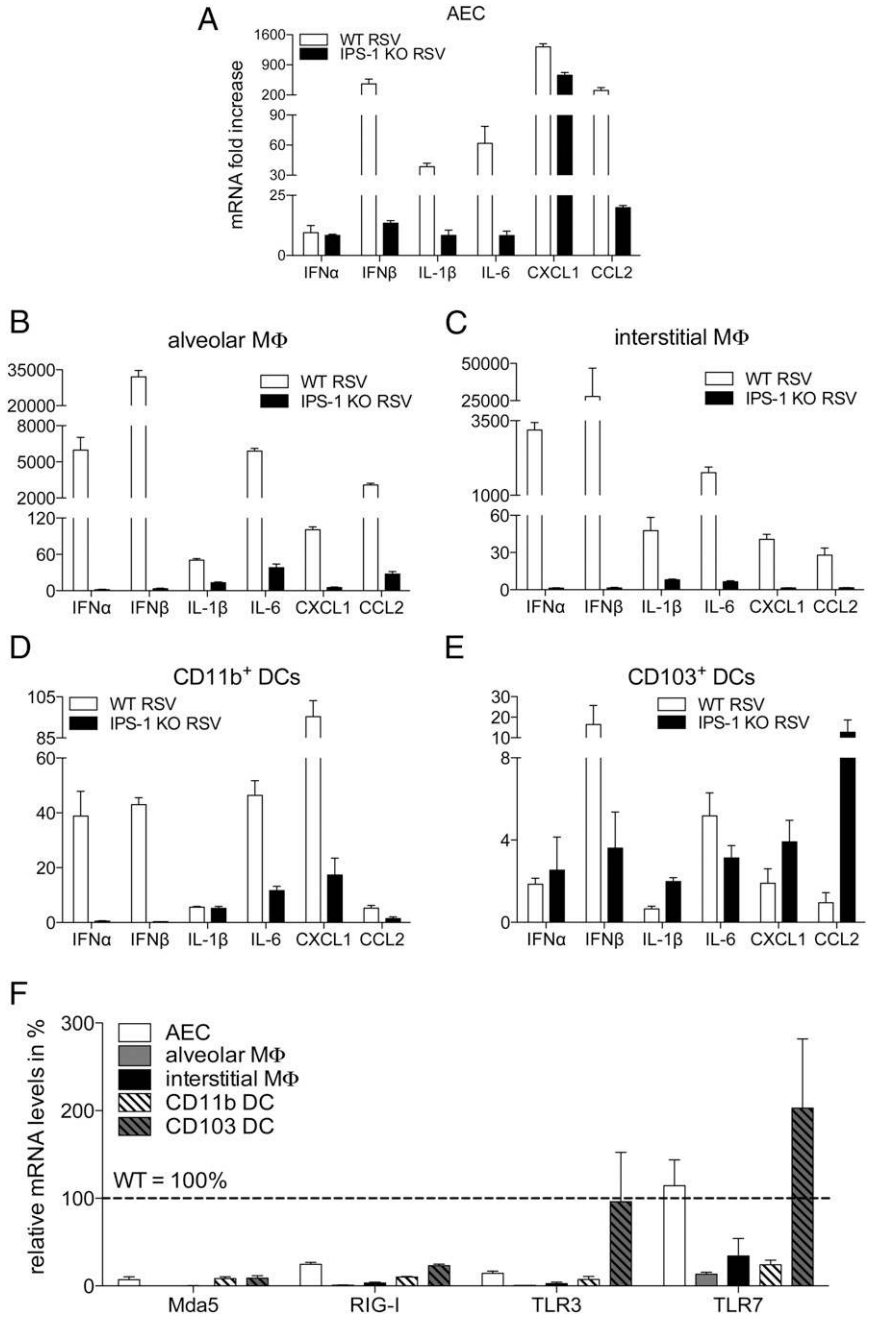

FIGURE 5. IPS-1 signaling mediates RSV-induced expression of cytokines, chemokines, and PRRs in the APCs of the lung. mRNA expression of IFN-α, IFN-β, IL-1β, IL-6, CXCL1, and CCL2 in primary cultures of AECs (**A**), alveolar MΦ (**B**), interstitial MΦ (**C**), pulmonary CD11b$^+$ (**D**), and CD103$^+$ DCs (**E**) isolated from WT versus IPS-1 KO lungs. (**F**) Overview of Mda5, RIG-I, TLR3, and TLR7 expression in different cell types of IPS-1 KO lungs, expressed as percentage of the mRNA levels observed in WT cells. All expression data are determined by RT-PCR 12 h postinfection with RSV (expressed as fold increase over controls; mean ± SEM; n = 4–5).

been identified as IFN-stimulated genes (20, 21). Interestingly, RSV-induced expression of IFN-α in CD103$^+$ DCs did not require IPS-1 signaling, and IL-1β, CXCL1, and CCL2 expression was enhanced in IPS-1 KO cells (Fig. 5E). Furthermore, IPS-1 KO CD103$^+$ DCs were able to upregulate TLR3 and TLR7 expression upon RSV infection (Fig. 5F). This observation suggests that CD103$^+$ DCs can functionally compensate for IPS-1 deficiency through detection of viral RNA via TLR3 and TLR7. In addition, the IPS-1–independent IFN-α induction in RSV-infected AECs may be driven by TLR7.

Differential regulation of inflammation and viral clearance by IPS-1 expression in immune and nonimmune cell populations

Given the different antiviral responses between AECs, structural cells, CD103$^+$ DCs, and hematopoietic cells, we next created bone marrow chimeras. This allowed us to address the question of whether IPS-1 signaling in either compartment, immune versus nonimmune, is crucial to control RSV-induced inflammation and viral clearance. Whereas RSV-induced inflammation was mostly cleared in WT → WT chimeras, peribronchiolar infiltrates could still be observed by day 8 post-RSV infection in mice with either IPS-1–deficient structural or hematopoietic cells (Fig. 6A). Moreover, inflammation appeared most persistent in syngeneic IPS-1 KO bone marrow chimeras, suggesting delayed resolution of RSV infection in these animals and recapitulation of the infection of nonchimerized KO animals. Accordingly, lung sections of KO → KO chimeras received the highest histopathology scores (4.0 ± 0.32; strong), which were significantly different from the scores for RSV-infected WT → WT chimeras (1.8 ± 0.37; slight) (Fig. 6B). In the case of allogeneic chimeras (KO → WT and WT → KO), the increase in pathology compared with WT → WT chimeras did not reach significance, supporting a partial rescue of the inflammation resolution in these animals. Looking at IFN-β mRNA levels in total lung, KO → KO chimeras had deficient IFN-β expression at 8 dpi, which is indeed rescued in KO → WT and WT → KO chimeras. We combined these results in a graph together with the histopathology scores (Fig. 6B), hereby illustrating that the dampened pulmonary IFN-β response is associated with greater inflammatory burden. In confirmation of the severe histopathology, high expression of the mRNAs coding for RSV F, G, and N proteins was still detected at 8 dpi in lungs of KO → KO chimeras, compared with WT → WT chimeras (Fig. 6C), whereas efficient elimination of RSV was observed in KO → WT or WT → KO chimeras. Thus, the overall response of deficient viral clearance with the most severe inflammation is only observed when both the immune and nonimmune compartments are deficient for IPS-1.

In the bone marrow chimera studies, we further characterized the inflammatory cell types infiltrating the lung during the antiviral response. Flow cytometric analysis indicated that airway infiltration with inflammatory neutrophils was increased in KO → KO chimeras and in WT → KO chimeras, albeit at a lower level (Fig. 7A, 7B), which may be explained the higher pulmonary expression of CCL3 and IL-17 in these chimeras (Fig. 7C). The airway neutrophilia was accompanied by elevated IFN-γ production in the mediastinal lymph nodes. IPS-1 deficiency in either hematopoietic or structural cells resulted in higher RSV-induced mRNA and protein levels of IFN-γ in restimulated lymph node cultures (Fig. 7D). Thus, IPS-1 deficiency in either the immune or nonimmune compartment sufficiently increased

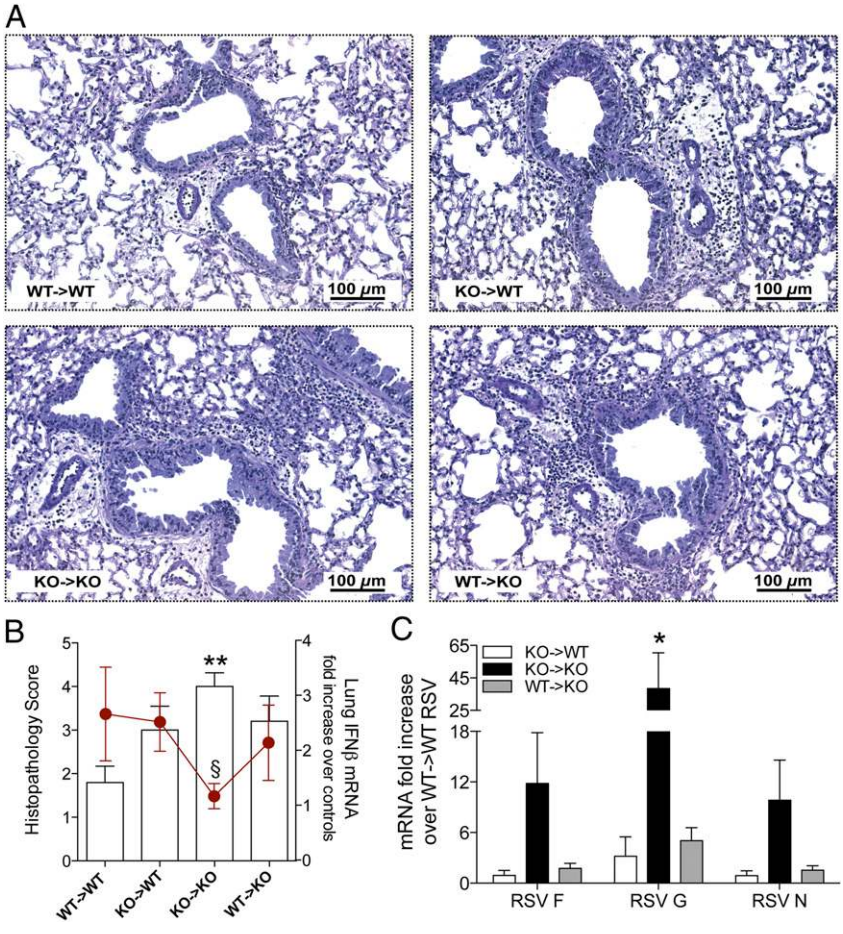

FIGURE 6. Most severe lung pathology in total absence of IPS-1 signaling, viral clearance rescued by IPS-1 expression in either immune or nonimmune cells. (**A**) Representative photomicrographs of hematoxylin-stained lung sections of WT → WT, KO → WT, KO → KO, and WT → KO chimeras at day 8 post-RSV infection. (**B**) Histopathology scores and mRNA expression of IFN-β (expressed as fold increase over WT → WT chimeras, mean ± SEM, $n = 5$). (**C**) mRNA expression of the RSV F, G, and N proteins in lungs of RSV-infected chimeras, as determined by RT-PCR on day 8 postinfection (expressed as fold increase over RSV-infected WT → WT chimeras, mean ± SEM, $n = 5$). $^*p < 0.05$, $^{**}p < 0.01$, $^{\S}p = 0.06$.

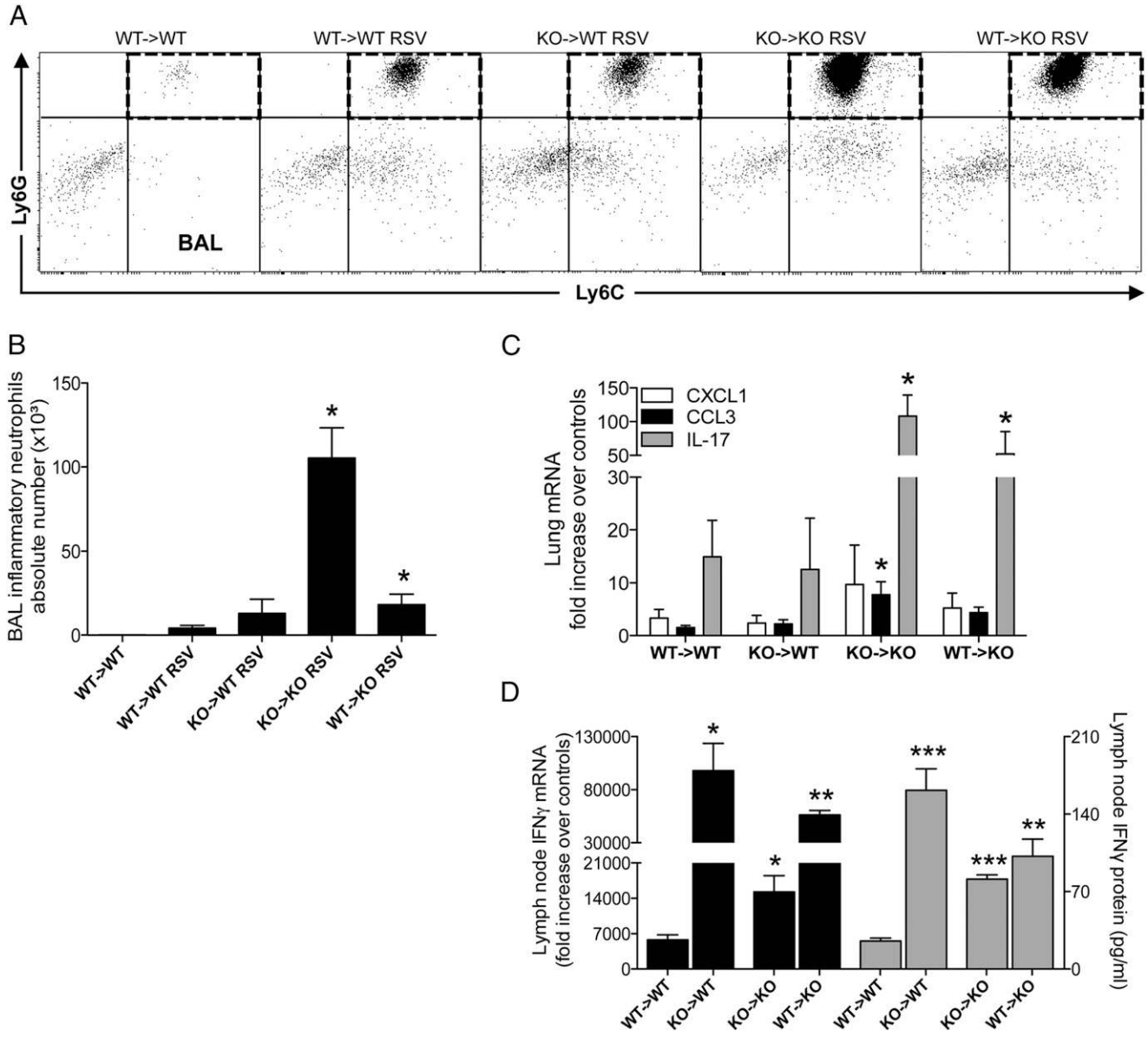

FIGURE 7. Most severe airway neutrophilia in total absence of IPS-1 signaling, IPS-1 deficiency in either structural or hematopoietic cells promotes an IFN-γ response in the lymph nodes. (**A**) Representative dot plots showing inflammatory neutrophils in the dashed quadrants ($Ly6C^{+}Ly6G^{hi}$, gated on $CD11c^{lo}$-low autofluorescent-$CD11b^{hi}$ population with low forward scatter) in the BAL fluid of naive WT → WT chimeras and RSV-infected WT → WT, KO → WT, KO → KO, and WT → KO chimeras. (**B**) Absolute numbers of BAL inflammatory neutrophils. (**C**) RSV-induced mRNA expression of CXCL1, CCL3, and IL-17 in lungs, determined by RT-PCR at 8 dpi (expressed as fold increase over WT → WT controls). (**D**) mRNA (expressed as fold increase over WT → WT controls) and protein (expressed as picograms per milliliter) levels of IFN-γ in restimulated cultures of mediastinal lymph nodes. All data are expressed as mean ± SEM, $n = 5$. $*p < 0.05$, $**p < 0.01$, $***p < 0.001$.

the lymph nodes responses, whereas a general IPS-1 defect was required for severe airway neutrophilia.

In addition to inflammatory neutrophils, we characterized the mononuclear cell populations accumulating in the lung upon RSV infection, using flow cytometry (Fig. 8A). In accordance with the airway neutrophilia, $CD11b^{hi}$ DCs accumulated in the airways and lungs of RSV-infected KO → KO and WT → KO chimeras (Fig. 8C, 8D). However, the proportion of newly recruited inflammatory ($Ly6C^{+}$) $CD11b^{hi}$ DCs was only increased when IPS-1 was absent in all cell types. Accordingly, RSV infection induced higher numbers of inflammatory monocytes, precursors for inflammatory $CD11b^{hi}$ DCs, only in lungs of syngeneic IPS-1 KO chimeras (Fig. 8B). In contrast, $CD103^{+}CD11b^{lo}$ DCs did not accumulate in lungs when IPS-1 signaling was hampered (data not shown). These infiltrating cells represent local cytokine/chemokine sources and RSV-targeted host cells, thus possibly adding to the delayed resolution of inflammation and RSV.

Discussion

This study highlights the importance of IPS-1 in generating the early IFN-β response upon RSV infection, as well as its nonredundant role in viral clearance. In lungs of IPS-1 KO mice, both structural and hematopoietic cells are hampered in their expression of RSV-induced inflammatory cytokines and chemokines. Nonetheless, IPS-1–deficient animals exhibit exaggerated bronchoalveolar and peribronchial inflammation, characterized by inflammatory $Ly6C^{+}$ neutrophils, $Ly6C^{+}$ monocytes, and $CD11b^{hi}$ $Ly6C^{+}$ DCs. Paradoxically, lymph node responses in RSV-infected IPS-1 KO mice are shifted toward a preferred Th1 cytokine profile, with Th1 and Tc cells exhibiting significant activation and

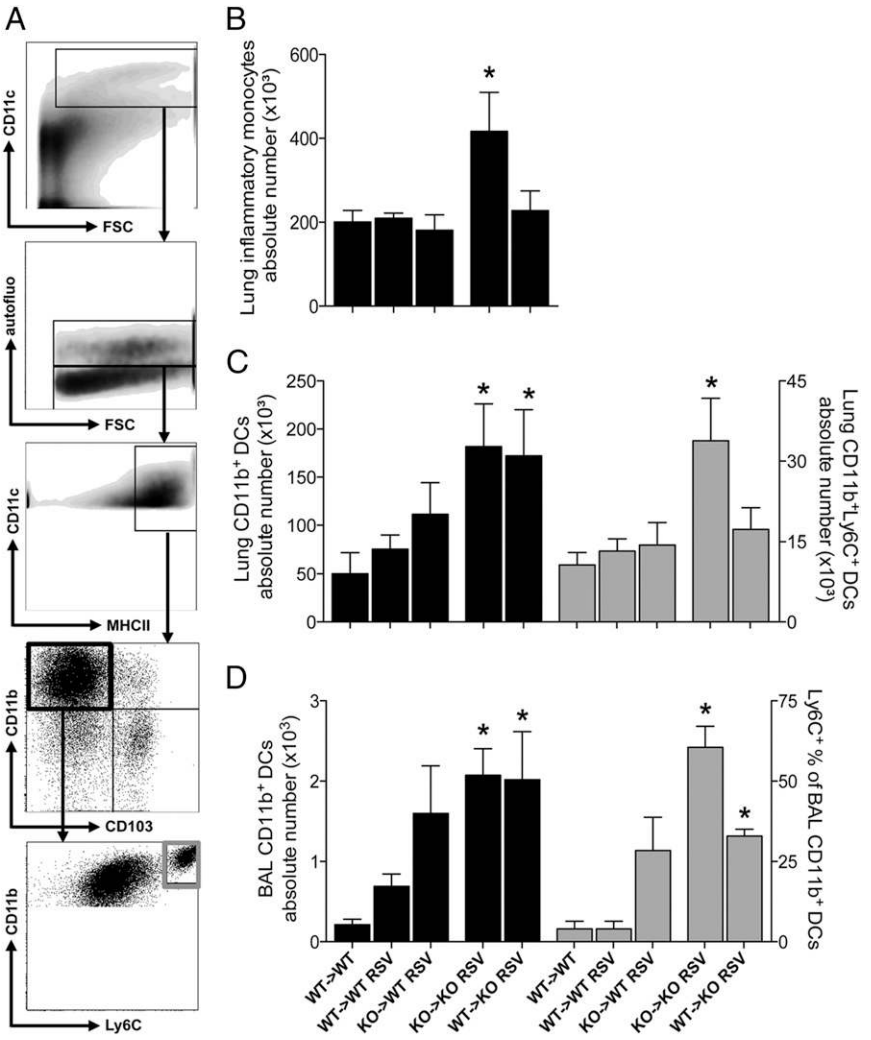

FIGURE 8. IPS-1 deficiency in structural cells induces CD11b$^+$ DC accumulation, inflammatory CD11b$^+$Ly6C$^+$ DCs and their monocytic precursors only infiltrate when all cells are IPS-1 deficient. (**A**) Pulmonary CD11b$^+$ DCs were defined as CD11c^{hi}MHCII$^+$CD11b^{hi}CD103$^-$ cells with low autofluorescence, inflammatory CD11b$^+$ DCs additionally expressed Ly6C. (**B**) Absolute numbers of pulmonary inflammatory monocytes (Ly6C$^+$Ly6G$^-$, gated on CD11c^{lo}-low autofluorescent-CD11b^{hi} population with low forward scatter). Numbers of total CD11b$^+$ DCs and inflammatory CD11b$^+$ DCs in lung tissue (**C**) and BAL fluid (**D**) of naive WT → WT chimeras and RSV-infected WT → WT, KO → WT, KO → KO, and WT → KO chimeras. All cell populations are analyzed by flow cytometry and expressed as mean ± SEM, $n = 5$. *$p < 0.05$.

IFN-γ production. In bone marrow chimeras, IPS-1 deficiency in nonimmune cells sufficiently increases cell infiltration into RSV-infected lungs, but the proinflammatory effect is maximal when IPS-1 signaling is absent in both structural and immune cells. In accordance, IPS-1 expression in either the nonimmune or the immune compartment adequately rescues viral clearance.

The blunted cytokine and chemokine response in IPS-1 KO AECs, pulmonary MΦ, and CD11b$^+$ DCs in vitro contrasts with the increased inflammation in RSV-infected IPS-1 KO mice in vivo. Even though the initial antiviral response may require IPS-1 activation, functional compensation likely occurs, considering the different pathways whereby the RSV genome can be detected. The preferred pathway for intracellular detection of viral RNA—endosomal via TLR3 and TLR7 versus cytoplasmic via RIG-I and Mda5—likely depends on the cell's ability to phagocytose and/or have a productive infection. In vitro studies previously demonstrated IPS-1–dependent induction of type I IFN by RSV in structural cells such as fibroblasts or in APCs including BMMΦ and BMDCs (9, 10). During the course of infection, TLR3 and TLR7 signaling will likely gain importance as apoptotic cells are phagocytized or when autophagy occurs within an infected host cell. Our in vitro data (Fig. 5D) as well as in vivo studies by others (10) strongly implicate IPS-1 signaling in the early RSV-induced activation (12–24 h postinfection) of CD11b$^+$ DCs. However, by 8 dpi, IPS-1 KO CD11b$^+$ DCs are both more abundant and more activated in infected lungs, suggesting a role for these cells in perpetuating the inflammatory response. Moreover, certain cell types in the lungs of IPS-1 KO mice may be initially skewed toward the generation of antiviral responses via the TLR3/TLR7 system. For instance, in our in vitro studies, pulmonary IPS-1–deficient CD103$^+$ DCs responded to RSV with the induction of TLR3 and TLR7, along with proinflammatory cytokines/chemokines, and thus emerged as potential orchestrators of inflammation. CD103$^+$ DC-derived CXCL1 and CCL2 may be responsible for the airway neutrophilia and monocytic infiltration in infected IPS-1 KO mice. This CD103$^+$ DC subset may also represent a previously described pulmonary DC subpopulation, which is activated in RSV-infected IPS-1 KO mice at 1 dpi (10). Similarly, CD8$^+$ DCs, the functional equivalent of CD103$^+$ DCs in lymphoid organs, have reduced expression of Mda5 and RIG-I in favor of TLR3, compared with other conventional DC populations in the spleen (22). Moreover, the RSV-induced TLR3 expression in migratory CD103$^+$ DCs may be advantageous for the generation of antiviral cytotoxic T cells in the lung-draining lymph nodes (23). It is also noteworthy that, despite several reports on hampered maturation of IPS-1 KO conventional DCs, IPS-1 KO BMMΦ and BMDCs can still secrete IL-12 upon RSV infection, albeit in lower levels compared with WT APCs (T. Demoor, unpublished observations).

In the absence of an initial systemic (in serum) and local (in BAL fluid) IFN-β response, we still observed increased T cell activation and IFN-γ production in IPS-1–deficient lungs locally, as well as in the mediastinal lymph nodes, complementing a previous report on increased IFN-γ levels in BAL fluid of RSV-infected IPS-1 KO

mice (10). Previous studies have shown that IPS-1 signaling dominantly controls the antiviral type I IFN response in nonhematopoietic cells (24). Interestingly, the lymph node IFN-γ response is most pronounced in a situation where the structural cells are IPS-1–competent but IPS-1–deficient hematopoietic cells are forced to compensate via TLR3/TLR7 signaling, demonstrated by our results in KO → WT chimeras. In addition to Th1 and Tc cells, the abundant neutrophils in RSV-infected IPS-1 KO are potential local sources for the IFN-γ levels observed in airways and lung tissue (25, 26). Moreover, aberrant immunosuppressive signals in IPS-1 KO mice may provide an additional explanation. RSV-infected IL-10 KO mice exhibit a comparable pattern of airway neutrophilia and inflammatory cytokines/chemokines in the presence of increased T cell-derived IFN-γ (27). Similarly, increased T cell numbers and IFN-γ expression upon infection of IPS-1 KO mice with West Nile virus were associated with uncontrolled inflammation and deficient regulatory T cell numbers (28).

The increased T_H1 and T_C cell response in the lymph nodes of IPS-1 KO animals is accompanied by deficient virus elimination. Whereas the TLR3 and TLR7 axis can maintain the cyto/chemokine response against RSV in certain cell types, the IFN stimulated genes Mda5 and RIG-I are reportedly essential to contain viral replication (29). In the absence of IPS-1 signaling, none of the pulmonary cell types we investigated in vitro could induce Mda5 or RIG-I upon RSV infection and accordingly, IPS-1–deficient animals showed defective viral clearance. Even though pDCs are vital to antiviral defense (30), using TLR7 for RSV detection (31), our findings in different pulmonary cell types of IPS-1 KO mice stress the importance of the alternative RIG-I–like detection system for efficient downstream immunity against RSV. Indeed, RSV-mediated TLR7 activation in pDCs is not determining for virus-induced type I IFN in our experiments: RSV appears as a poor inducer of IFN-α, and the local and systemic levels of IFN-β depend on IPS-1 signaling. However, pDC numbers were significantly increased in lungs of RSV-infected WT but not IPS-1 KO mice (Supplemental Fig. 4B). Also, splenic pDCs have been described to express both Mda5 and RIG-I (22), motivating a revisit of viral recognition in pulmonary pDCs. In addition, both structural AECs as well as pulmonary MΦ are likely to generate the early type I IFN response and effective antiviral responses in an IPS-1–dependent fashion. Accordingly, IPS-1 expression in either nonimmune or immune cells rescues both the inflammatory phenotype and the viral clearance for the greater part.

The adaptive immune cells in IPS-1–deficient animals are possibly overwhelmed by the excessive influx of innate cells, representing additional host cells for RSV infection. Persisting inflammation and viral replication could maintain each other but may be affected by a third process, apoptosis. Apoptosis may contribute to an efficient antiviral defense: first, when cellular suicide stops viral replication; second, when infiltrated inflammatory cells undergo apoptosis and are engulfed during the resolution phase. The nonstructural RSV proteins (NS1 and NS2) for instance have been shown to delay apoptosis, thus promoting viral growth (32). NS1 and NS2 reportedly target RIG-I to inhibit its downstream interaction with IPS-1 (33, 34). The mitochondrial localization of IPS-1 together with its caspase activation and recruitment domain suggests a role for IPS-1 in mitochondrion-dependent apoptotic pathways. Accordingly, IPS-1 is required for apoptosis of mouse embryonic fibroblasts infected with Sendai virus (35, 36). Altered apoptosis in the absence of IPS-1 may explain the exaggerated inflammation and the contradicting observation of increased Th1 and T_C activation yet reduced viral clearance. In previous reports on normal RSV-specific Tc cells in IPS-1 KO mice (10), these cells may thus be hampered in their cytolytic elimination of RSV-infected cells. In addition to being a stimulator of early IFN-β induction, the potential regulation of apoptosis by IPS-1 adds complexity to its role in antiviral responses.

In conclusion, our data support a nonredundant role for IPS-1 in controlling RSV-induced inflammation and viral replication. Our findings regarding the targeting of RIG-like helicases versus TLRs by RSV, respectively, in the nonimmune and immune cells of the lung provide crucial information for the ongoing development of a vaccine against RSV.

Acknowledgments

We thank Judith Connett (Department of Pathology, University of Michigan, Ann Arbor, MI) for editing the manuscript and Aaron Berlin (Department of Pathology, University of Michigan, Ann Arbor, MI) for excellent technical assistance.

Disclosures

The authors have no financial conflicts of interest.

References

1. Rudd, B. D., J. J. Smit, R. A. Flavell, L. Alexopoulou, M. A. Schaller, A. Gruber, A. A. Berlin, and N. W. Lukacs. 2006. Deletion of TLR3 alters the pulmonary immune environment and mucus production during respiratory syncytial virus infection. *J. Immunol.* 176: 1937–1942.
2. Lukacs, N. W., J. J. Smit, S. Mukherjee, S. B. Morris, G. Nunez, and D. M. Lindell. 2010. Respiratory virus-induced TLR7 activation controls IL-17-associated increased mucus via IL-23 regulation. *J. Immunol.* 185: 2231–2239.
3. Sabbah, A., T. H. Chang, R. Harnack, V. Frohlich, K. Tominaga, P. H. Dube, Y. Xiang, and S. Bose. 2009. Activation of innate immune antiviral responses by Nod2. *Nat. Immunol.* 10: 1073–1080.
4. Hornung, V., J. Ellegast, S. Kim, K. Brzózka, A. Jung, H. Kato, H. Poeck, S. Akira, K. K. Conzelmann, M. Schlee, et al. 2006. 5′-Triphosphate RNA is the ligand for RIG-I. *Science* 314: 994–997.
5. Pichlmair, A., O. Schulz, C. P. Tan, T. I. Näslund, P. Liljeström, F. Weber, and C. Reis e Sousa. 2006. RIG-I-mediated antiviral responses to single-stranded RNA bearing 5′-phosphates. *Science* 314: 997–1001.
6. Kawai, T., K. Takahashi, S. Sato, C. Coban, H. Kumar, H. Kato, K. J. Ishii, O. Takeuchi, and S. Akira. 2005. IPS-1, an adaptor triggering RIG-I- and Mda5-mediated type I interferon induction. *Nat. Immunol.* 6: 981–988.
7. Seth, R. B., L. Sun, C. K. Ea, and Z. J. Chen. 2005. Identification and characterization of MAVS, a mitochondrial antiviral signaling protein that activates NF-κB and IRF 3. *Cell* 122: 669–682.
8. Jafri, H. S., S. Chavez-Bueno, A. Mejias, A. M. Gomez, A. M. Rios, S. S. Nassi, M. Yusuf, P. Kapur, R. D. Hardy, J. Hatfield, et al. 2004. Respiratory syncytial virus induces pneumonia, cytokine response, airway obstruction, and chronic inflammatory infiltrates associated with long-term airway hyperresponsiveness in mice. *J. Infect. Dis.* 189: 1856–1865.
9. Loo, Y. M., J. Fornek, N. Crochet, G. Bajwa, O. Perwitasari, L. Martinez-Sobrido, S. Akira, M. A. Gill, A. García-Sastre, M. G. Katze, and M. Gale, Jr. 2008. Distinct RIG-I and MDA5 signaling by RNA viruses in innate immunity. *J. Virol.* 82: 335–345.
10. Bhoj, V. G., Q. Sun, E. J. Bhoj, C. Somers, X. Chen, J. P. Torres, A. Mejias, A. M. Gomez, H. Jafri, O. Ramilo, and Z. J. Chen. 2008. MAVS and MyD88 are essential for innate immunity but not cytotoxic T lymphocyte response against respiratory syncytial virus. *Proc. Natl. Acad. Sci. USA* 105: 14046–14051.
11. Kumar, H., T. Kawai, H. Kato, S. Sato, K. Takahashi, C. Coban, M. Yamamoto, S. Uematsu, K. J. Ishii, O. Takeuchi, and S. Akira. 2006. Essential role of IPS-1 in innate immune responses against RNA viruses. *J. Exp. Med.* 203: 1795–1803.
12. Lukacs, N. W., M. L. Moore, B. D. Rudd, A. A. Berlin, R. D. Collins, S. J. Olson, S. B. Ho, and R. S. Peebles, Jr. 2006. Differential immune responses and pulmonary pathophysiology are induced by two different strains of respiratory syncytial virus. *Am. J. Pathol.* 169: 977–986.
13. Mendez, M. P., S. B. Morris, S. Wilcoxen, M. Du, Y. K. Monroy, H. Remmer, H. Murphy, P. J. Christensen, and R. Paine, III. 2008. Disparate mechanisms of sICAM-1 production in the peripheral lung: contrast between alveolar epithelial cells and pulmonary microvascular endothelial cells. *Am. J. Physiol. Lung Cell. Mol. Physiol.* 294: L807–L814.
14. Demoor, T., K. R. Bracke, L. L. Dupont, M. Plantinga, B. Bondue, M. O. Roy, V. Lannoy, B. N. Lambrecht, G. G. Brusselle, and G. F. Joos. 2011. The role of ChemR23 in the induction and resolution of cigarette smoke-induced inflammation. *J. Immunol.* 186: 5457–5467.
15. Miller, A. L., T. L. Bowlin, and N. W. Lukacs. 2004. Respiratory syncytial virus-induced chemokine production: linking viral replication to chemokine production in vitro and in vivo. *J. Infect. Dis.* 189: 1419–1430.
16. Diebold, S. S., T. Kaisho, H. Hemmi, S. Akira, and C. Reis e Sousa. 2004. Innate antiviral responses by means of TLR7-mediated recognition of single-stranded RNA. *Science* 303: 1529–1531.
17. Lund, J. M., L. Alexopoulou, A. Sato, M. Karow, N. C. Adams, N. W. Gale, A. Iwasaki, and R. A. Flavell. 2004. Recognition of single-stranded RNA viruses by Toll-like receptor 7. *Proc. Natl. Acad. Sci. USA* 101: 5598–5603.

18. Kato, H., O. Takeuchi, S. Sato, M. Yoneyama, M. Yamamoto, K. Matsui, S. Uematsu, A. Jung, T. Kawai, K. J. Ishii, et al. 2006. Differential roles of MDA5 and RIG-I helicases in the recognition of RNA viruses. *Nature* 441: 101–105.
19. Liu, P., M. Jamaluddin, K. Li, R. P. Garofalo, A. Casola, and A. R. Brasier. 2007. Retinoic acid-inducible gene I mediates early antiviral response and Toll-like receptor 3 expression in respiratory syncytial virus-infected airway epithelial cells. *J. Virol.* 81: 1401–1411.
20. Kang, D. C., R. V. Gopalkrishnan, Q. Wu, E. Jankowsky, A. M. Pyle, and P. B. Fisher. 2002. mda-5: An interferon-inducible putative RNA helicase with double-stranded RNA-dependent ATPase activity and melanoma growth-suppressive properties. *Proc. Natl. Acad. Sci. USA* 99: 637–642.
21. Yoneyama, M., M. Kikuchi, T. Natsukawa, N. Shinobu, T. Imaizumi, M. Miyagishi, K. Taira, S. Akira, and T. Fujita. 2004. The RNA helicase RIG-I has an essential function in double-stranded RNA-induced innate antiviral responses. *Nat. Immunol.* 5: 730–737.
22. Luber, C. A., J. Cox, H. Lauterbach, B. Fancke, M. Selbach, J. Tschopp, S. Akira, M. Wiegand, H. Hochrein, M. O'Keeffe, and M. Mann. 2010. Quantitative proteomics reveals subset-specific viral recognition in dendritic cells. *Immunity* 32: 279–289.
23. Schulz, O., S. S. Diebold, M. Chen, T. I. Näslund, M. A. Nolte, L. Alexopoulou, Y. T. Azuma, R. A. Flavell, P. Liljeström, and C. Reis e Sousa. 2005. Toll-like receptor 3 promotes cross-priming to virus-infected cells. *Nature* 433: 887–892.
24. Schilte, C., M. R. Buckwalter, M. E. Laird, M. S. Diamond, O. Schwartz, and M. L. Albert. 2012. Cutting edge: independent roles for IRF-3 and IRF-7 in hematopoietic and nonhematopoietic cells during host response to Chikungunya infection. *J. Immunol.* 188: 2967–2971.
25. Yin, J., and T. A. Ferguson. 2009. Identification of an IFN-gamma-producing neutrophil early in the response to *Listeria monocytogenes*. *J. Immunol.* 182: 7069–7073.
26. Yamada, M., J. C. Gomez, P. E. Chugh, C. A. Lowell, M. C. Dinauer, D. P. Dittmer, and C. M. Doerschuk. 2011. Interferon-γ production by neutrophils during bacterial pneumonia in mice. *Am. J. Respir. Crit. Care Med.* 183: 1391–1401.
27. Loebbermann, J., C. Schnoeller, H. Thornton, L. Durant, N. P. Sweeney, M. Schuijs, A. O'Garra, C. Johansson, and P. J. Openshaw. 2012. IL-10 regulates viral lung immunopathology during acute respiratory syncytial virus infection in mice. *PLoS One* 7: e32371.
28. Suthar, M. S., D. Y. Ma, S. Thomas, J. M. Lund, N. Zhang, S. Daffis, A. Y. Rudensky, M. J. Bevan, E. A. Clark, M. K. Kaja, et al. 2010. IPS-1 is essential for the control of West Nile virus infection and immunity. *PLoS Pathog.* 6: e1000757.
29. Schoggins, J. W., S. J. Wilson, M. Panis, M. Y. Murphy, C. T. Jones, P. Bieniasz, and C. M. Rice. 2011. A diverse range of gene products are effectors of the type I interferon antiviral response. *Nature* 472: 481–485.
30. Smit, J. J., B. D. Rudd, and N. W. Lukacs. 2006. Plasmacytoid dendritic cells inhibit pulmonary immunopathology and promote clearance of respiratory syncytial virus. *J. Exp. Med.* 203: 1153–1159.
31. Gilliet, M., W. Cao, and Y. J. Liu. 2008. Plasmacytoid dendritic cells: sensing nucleic acids in viral infection and autoimmune diseases. *Nat. Rev. Immunol.* 8: 594–606.
32. Bitko, V., O. Shulyayeva, B. Mazumder, A. Musiyenko, M. Ramaswamy, D. C. Look, and S. Barik. 2007. Nonstructural proteins of respiratory syncytial virus suppress premature apoptosis by an NF-κB-dependent, interferon-independent mechanism and facilitate virus growth. *J. Virol.* 81: 1786–1795.
33. Ling, Z., K. C. Tran, and M. N. Teng. 2009. Human respiratory syncytial virus nonstructural protein NS2 antagonizes the activation of beta interferon transcription by interacting with RIG-I. *J. Virol.* 83: 3734–3742.
34. Boyapalle, S., T. Wong, J. Garay, M. Teng, H. San Juan-Vergara, S. Mohapatra, and S. Mohapatra. 2012. Respiratory syncytial virus NS1 protein colocalizes with mitochondrial antiviral signaling protein MAVS following infection. *PLoS One* 7: e29386.
35. Lei, Y., C. B. Moore, R. M. Liesman, B. P. O'Connor, D. T. Bergstralh, Z. J. Chen, R. J. Pickles, and J. P. Ting. 2009. MAVS-mediated apoptosis and its inhibition by viral proteins. *PLoS One* 4: e5466.
36. Chattopadhyay, S., J. T. Marques, M. Yamashita, K. L. Peters, K. Smith, A. Desai, B. R. Williams, and G. C. Sen. 2010. Viral apoptosis is induced by IRF-3-mediated activation of Bax. *EMBO J.* 29: 1762–1773.